Optics Letters

Ultimate conversion efficiency bound for the forward double-Λ atom–light coupling scheme

Dionisis Stefanatos,[1,*] **Athanasios Smponias,**[1] **Hamid Reza Hamedi,**[2] and **Emmanuel Paspalakis**[1]

[1]*Materials Science Department, School of Natural Sciences, University of Patras, Patras 26504, Greece*
[2]*Institute of Theoretical Physics and Astronomy, Vilnius University, Saulėtekio 3, Vilnius LT-10257, Lithuania*
Corresponding author: dionisis@post.harvard.edu

We show that for the two widely used configurations of the double-Λ atom–light coupling scheme, one where the control fields are applied in the same Λ-subsystem and another where they are applied in different Λ-subsystems, the forward propagation of the probe and signal fields is described by the same set of equations. We then use optimal control theory to find the spatially dependent optimal control fields that maximize the conversion efficiency from the probe to the signal field, for a given optical density. This work can find application in the implementation of efficient frequency and orbital angular momentum conversion devices for quantum information processing, as well as to be useful for many other applications using the double-Λ atom–light coupling scheme. © 2020 Optical Society of America

https://doi.org/10.1364/OL.404173

During the last few decades, the double-Λ atom–light coupling scheme [1] has received considerable attention among the quantum optics community. This system is a four-state unbranched loop where the labeling of the four applied laser fields can be considered as two linked Λ-subsystems, as shown in Fig. 1. Usually, a pair of strong control fields Ω_c, Ω_d, which can be spatially dependent, prepares atoms in a coherent superposition state. This coherently prepared atomic cloud can be used to manipulate the properties of the weak probe and signal fields Ω_p, Ω_s propagating inside it. For example, when the signal field is absent at the entrance to the medium, this setup can generate it by converting the probe field.

The double-Λ atom–light coupling scheme finds a wide range of applications, including light storage [3,4], generation of squeezed light states [5,6], phase-controlled light switching [7,8], frequency conversion [9–17], and orbital angular momentum conversion [18–21] between light beams, as well as many others [2,22–27]. In most of these works, two configurations of the applied laser fields are usually encountered. In the first, which we call the direct configuration and display in Fig. 1(a), the probe and signal fields appear in the same Λ-subsystem, while the control fields are applied in the other. In the other configuration, shown in Fig. 1(b), the probe and

signal fields appear in different Λ-subsystems; we call this the mixed configuration.

In the present work, we show that, under some reasonable approximations, the forward propagation of the probe and signal fields in both configurations is described by the same set of equations. Then, we use optimal control theory [28] to find the optimal control fields Ω_c, Ω_d that maximize the conversion efficiency from Ω_p to Ω_s for a given optical density. We emphasize that we concentrate on the forward scheme, where Ω_p, Ω_s propagate in the same direction, which suffers less from phase mismatch than the backward propagation scheme [17]. Also, we consider the case where all fields are resonant with the corresponding transitions, so the interaction strength between atoms and photons is maximized.

We consider first the mixed configuration, shown in Fig. 1(b). The Maxwell–Bloch equations governing the dynamics of the fields Ω_p, Ω_s and the atomic coherences ρ_{21}, ρ_{31}, ρ_{41} are [17]

$$\frac{d}{dt}\rho_{31} = i(\Omega_p + \Omega_c \rho_{21}) - \Gamma_{31}\rho_{31}, \tag{1a}$$

$$\frac{d}{dt}\rho_{41} = i(\Omega_s + \Omega_d \rho_{21}) - \Gamma_{41}\rho_{41}, \tag{1b}$$

$$\frac{d}{dt}\rho_{21} = i(\Omega_c^* \rho_{31} + \Omega_d^* \rho_{41}) - \Gamma_{21}\rho_{21}, \tag{1c}$$

and

$$\frac{\partial}{\partial z}\Omega_p + \frac{1}{c}\frac{\partial}{\partial t}\Omega_p = i\frac{\alpha_p \Gamma_{31}}{2L}\rho_{31}, \tag{2a}$$

$$\frac{\partial}{\partial z}\Omega_s + \frac{1}{c}\frac{\partial}{\partial t}\Omega_s = i\frac{\alpha_s \Gamma_{41}}{2L}\rho_{41}, \tag{2b}$$

where Γ_{31}, Γ_{41} are the spontaneous decay rates of the excited states, Γ_{21} is the dephasing rate of the ground states, α_p, α_s are, respectively, the optical densities of the probe and signal transitions, and L is the length of the medium. To simplify the model, we assume $\Gamma_{31} = \Gamma_{41} = \Gamma$, $\Gamma_{21} = 0$, and $\alpha_p = \alpha_s = \alpha$, justified in Refs. [17,19,20]. Note also that in Eq. (1), we use the approximation $\rho_{11} \approx 1$, which is valid to first order for
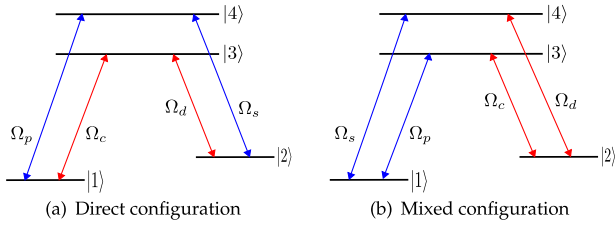
Fig. 1. (a) In the direct configuration, the probe and signal fields Ω_p, Ω_s appear in the same Λ-subsystem, while the control fields Ω_c, Ω_d are applied in the other. (b) In the mixed configuration, the probe and signal fields appear in different Λ-subsystems. This configuration can also be viewed as built by a Λ- and a V-system [2].

weak probe and signal fields. If we solve for the steady state of system (1), we get to the first order (see Supplement 1):

$$\begin{pmatrix} \rho_{31} \\ \rho_{41} \end{pmatrix} = \frac{i}{\Gamma} \begin{pmatrix} \cos^2 \theta & -\sin \theta \cos \theta \\ -\sin \theta \cos \theta & \sin^2 \theta \end{pmatrix} \begin{pmatrix} \Omega_p \\ \Omega_s \end{pmatrix}, \quad \textbf{(3)}$$

where θ is the mixing angle defined by the equation

$$\Omega_c = \Omega \sin \theta, \quad \Omega_d = \Omega \cos \theta, \quad \textbf{(4)}$$

Ω being the generalized Rabi frequency. Substituting Eq. (3) into Eq. (2), we obtain in the steady state the following coupled equations for the propagation of the probe and signal pulses:

$$\frac{\partial}{\partial z} \begin{pmatrix} \Omega_p \\ \Omega_s \end{pmatrix} = -\frac{\alpha}{2L} \begin{pmatrix} \cos^2 \theta & -\sin \theta \cos \theta \\ -\sin \theta \cos \theta & \sin^2 \theta \end{pmatrix} \begin{pmatrix} \Omega_p \\ \Omega_s \end{pmatrix}. \quad \textbf{(5)}$$

The above system, which describes pulse propagation for the mixed configuration, is exactly the same as the corresponding system for the direct configuration, derived in Refs. [19,20]. If we normalize the propagation distance z with the absorption length $L_{abs} = L/\alpha$ and use the dimensionless variable $\zeta = z/L_{abs}$, we get

$$\begin{pmatrix} \dot{\Omega}_p \\ \dot{\Omega}_s \end{pmatrix} = -\frac{1}{2} \begin{pmatrix} \cos^2 \theta & -\sin \theta \cos \theta \\ -\sin \theta \cos \theta & \sin^2 \theta \end{pmatrix} \begin{pmatrix} \Omega_p \\ \Omega_s \end{pmatrix}, \quad \textbf{(6)}$$

where the dot denotes the derivative $\partial/\partial\zeta$. Under this transformation, the propagation takes place from $\zeta = 0$ to $\zeta = \alpha$.

In order to study pulse propagation under a position-dependent mixing angle $\theta(\zeta)$, i.e., spatially varying control fields $\Omega_c(\zeta), \Omega_d(\zeta)$, it is more convenient to work in the adiabatic frame. The eigenstates of the propagation matrix in Eq. (6) are

$$\psi_0 = \begin{pmatrix} \sin \theta \\ \cos \theta \end{pmatrix}, \quad \psi_{-1/2} = \begin{pmatrix} \cos \theta \\ -\sin \theta \end{pmatrix}, \quad \textbf{(7)}$$

with corresponding eigenvalues zero and $-1/2$, respectively. The transformation to the adiabatic basis is

$$\begin{pmatrix} y \\ x \end{pmatrix} = \begin{pmatrix} \sin \theta & \cos \theta \\ \cos \theta & -\sin \theta \end{pmatrix} \begin{pmatrix} \Omega_p \\ \Omega_s \end{pmatrix}. \quad \textbf{(8)}$$

Using Eqs. (6) and (8), we find

$$\begin{pmatrix} \dot{y} \\ \dot{x} \end{pmatrix} = \begin{pmatrix} 0 & -u \\ u & -\frac{1}{2} \end{pmatrix} \begin{pmatrix} y \\ x \end{pmatrix}, \quad \textbf{(9)}$$

where the control function $u(\zeta)$ is defined as

$$\dot{\theta} = -u. \quad \textbf{(10)}$$

For $\Omega_p(0) = \Omega_0, \Omega_s(0) = 0$ and the boundary conditions

$$\theta(0) = \frac{\pi}{2}, \quad \theta(\alpha) = 0, \quad \textbf{(11)}$$

we get

$$x(0) = 0, \quad y(0) = \Omega_p(0) = \Omega_0, \quad \textbf{(12)}$$

and

$$x(\alpha) = \Omega_p(\alpha), \quad y(\alpha) = \Omega_s(\alpha). \quad \textbf{(13)}$$

It is worth pointing out that for large α, if θ varies slowly between the values in Eq. (11), with rate $u = |\dot{\theta}| \ll 1$, then $y(\zeta)$ remains constant during the evolution, and thus $\Omega_s(\alpha) = y(\alpha) \approx y(0) = \Omega_p(0) = \Omega_0$. The slow conversion from the initial Ω_p to the final Ω_s takes place along the eigenstate ψ_0 of the original system (6).

We next move to find the optimal control $u(\zeta)$, $0 \le \zeta \le \alpha$, for given finite optical density α, which maximizes the final value $\Omega_s(\alpha) = y(\alpha)$. The control Hamiltonian is [28]

$$H_c = \lambda_x \dot{x} + \lambda_y \dot{y} + \mu u = (\lambda_x y - \lambda_y x + \mu)u - \frac{1}{2}\lambda_x x, \quad \textbf{(14)}$$

where $\lambda_x, \lambda_y, \mu$ are the Lagrange multipliers corresponding to x, y, θ. They satisfy the adjoint equations

$$\dot{\lambda}_y = -\frac{\partial H_c}{\partial y} = -u\lambda_x, \quad \textbf{(15a)}$$

$$\dot{\lambda}_x = -\frac{\partial H_c}{\partial x} = u\lambda_y + \frac{1}{2}\lambda_x, \quad \textbf{(15b)}$$

while μ is constant since θ is a cyclic variable. The optimal control $u(\zeta)$ is chosen to maximize the control Hamiltonian H_c [28], which is a mathematical construction, so its maximization does not correspond to maximizing the energy of some system but the target quantity $y(\alpha)$. Note that we have not imposed any bound on u, so Eqs. (9) and (10) are fully equivalent to the original system (6). Even infinite values are allowed momentarily, corresponding to instantaneous jumps in the angle θ. Since H_c is a linear function of u with coefficient $\phi = \lambda_x y - \lambda_y x + \mu$, if $\phi \neq 0$ for a finite interval, then the corresponding optimal control should be $\pm\infty$ for the whole interval, which is obviously unphysical. We conclude that $\phi = 0$ almost everywhere, except some isolated points where jumps in the angle θ can occur. The optimal control that maintains this condition is called *singular* [28]. Such controls have been exploited in nuclear magnetic resonance to minimize the effect of relaxation [29]. In order to find the singular optimal control u_s, we additionally use the conditions $\dot{\phi} = \ddot{\phi} = 0$ and obtain the following equations:

$$\lambda_y x - \lambda_x y = \mu, \quad \textbf{(16a)}$$

$$\lambda_y x + \lambda_x y = 0, \quad \textbf{(16b)}$$

$$2(\lambda_y y - \lambda_x x)u_s = \frac{1}{2}(\lambda_x x - \lambda_x y). \quad \textbf{(16c)}$$

Solving for λ_x, λ_y, u_s, we find

$$\lambda_x = -\frac{\mu}{2y}, \quad \lambda_y = \frac{\mu}{2x}, \tag{17}$$

$$u_s = \frac{xy}{2(x^2 + y^2)}. \tag{18}$$

According to optimal control theory [28], the control Hamiltonian for a system without explicit dependence on the running variable ζ, as in our case, is constant. Using $\phi = 0$ and Eq. (17) for λ_x in Eq. (14), we conclude that the singular arc is a straight line passing through the origin of xy plane:

$$\frac{y}{x} = \text{const.} = \tan\theta_0. \tag{19}$$

This implies that the singular control u_s, given in Eq. (18) in terms of a feedback law, is also constant. Now we can describe the optimal pulse sequence. There is a delta pulse at $\zeta = 0$, resulting in a jump from $\theta(0^-) = \pi/2$ to $\theta(0^+) = \theta_0$, where the initial angle is to be determined. The system is brought on the singular arc and remains there for $0 < \zeta < \alpha$. During this interval, the angle decreases linearly with slope u_s, $\theta(\zeta) = \theta_0 - u_s\zeta$. At the final distance $\zeta = \alpha$, another delta pulse changes the angle from $\theta(\alpha^-) = \theta_0 - u_s\alpha$ to $\theta(\alpha^+) = 0$. The optimal control has the form *bang-singular-bang*:

$$u(\zeta) = \begin{cases} (\pi/2 - \theta_0)\delta(\zeta), & \zeta = 0 \\ u_s, & 0 < \zeta < \alpha \\ (\theta_0 - u_s\alpha)\delta(\zeta - \alpha), & \zeta = a \end{cases}. \tag{20}$$

Observe from the original system (6) that jumps in the angle θ do not change Ω_p, Ω_s. In the adiabatic basis, these jumps are accompanied by sudden rotations of the $(x, y)^T$ vector such that Ω_p, Ω_s remain unchanged [see transformation (8)]. Thus, in order to implement the optimal protocol, one simply needs to vary linearly the angle from θ_0 to $\theta_0 - u_s\alpha$ with the slope $u_s < \pi/(2\alpha)$.

We now find the optimal θ_0 corresponding to a given optical density α. After the application of the pulse sequence (20) to system (9), we get

$$\frac{|\Omega_s(\alpha)|^2}{|\Omega_0|^2} = e^{-2\gamma\alpha}\sin^2(u_s\alpha), \tag{21}$$

where

$$u_s = \frac{\tan\theta_0}{2(1 + \tan^2\theta_0)} = \frac{1}{4}\sin(2\theta_0) \tag{22}$$

from Eqs. (18) and (19), and

$$\gamma = \frac{1}{2(1 + \tan^2\theta_0)}. $$

Optimizing Eq. (21) with respect to θ_0, we get

$$\tan(u_s\alpha) = \frac{du_s}{d\theta_0} \Big/ \frac{d\gamma}{d\theta_0} = \frac{\tan^2\theta_0 - 1}{2\tan\theta_0} = \tan\left(2\theta_0 - \frac{\pi}{2}\right). \tag{23}$$

Since $0 < u_s\alpha < \pi/2$ and $\pi/4 < \theta_0 < \pi/2$, where the lower bound in the latter relation comes from the third term in Eq. (23), from the monotonicity of the tan function in $(0, \pi/2)$, we conclude that

$$\frac{\alpha}{4}\sin(2\theta_0) = 2\theta_0 - \frac{\pi}{2}, \tag{24}$$

where we have also used Eq. (22). For a given optical density α, this is a transcendental equation for θ_0. It can be easily proved that it has a unique solution in the interval $\pi/4 < \theta_0 < \pi/2$. Note that for $\alpha \to 0$, it is $\theta_0 \to \pi/4$, while for $\alpha \to \infty$, it is $\theta_0 \to \pi/2$. The limiting values of the optimal conversion efficiency are

$$\frac{|\Omega_s(\alpha)|^2}{|\Omega_0|^2} = \begin{cases} \frac{1}{16}\alpha^2, & \alpha \ll 1 \\ 1 - \frac{\pi^2}{\alpha}, & \alpha \gg 1 \end{cases}, \tag{25}$$

and thus for sufficiently large optical density, the conversion efficiency approaches unity. In Fig. 2, we plot the optimal conversion efficiency (red solid line) as a function of the optical density, for $0 \le \alpha \le 100$.

As we pointed out above, for large α, we have $\theta_0 \to \pi/2$, and thus the boundary jumps become smaller. In this limit, the optimal solution tends to a linear decrease of the angle θ from $\pi/2$ to zero:

$$u(\zeta) = \text{const.} = \frac{\pi}{2\alpha}, \quad \theta(\zeta) = \frac{\pi}{2} - u\zeta. \tag{26}$$

Under this constant control protocol, ensuring that $\Omega_c(0) = \Omega_d(\alpha) = \Omega_0$ and $\Omega_c(\alpha) = \Omega_d(0) = 0$, Eq. (9) can be easily integrated, and at the final distance $\zeta = \alpha$, one finds [15,17]

$$\frac{|\Omega_s(\alpha)|^2}{|\Omega_0|^2} = e^{-\eta\alpha}\left[\cosh(\kappa\alpha) + \frac{\eta}{2\kappa}\sinh(\kappa\alpha)\right]^2, \tag{27}$$

where

$$\eta = \frac{1}{2}, \quad \kappa = \sqrt{\left(\frac{\eta}{2}\right)^2 - u^2}. $$

From Eq. (27), we find the limiting cases

$$\frac{|\Omega_s(\alpha)|^2}{|\Omega_0|^2} = \begin{cases} \frac{1}{4\pi^2}\alpha^2, & \alpha \ll 1 \\ 1 - \frac{\pi^2}{\alpha}, & \alpha \gg 1 \end{cases}. \tag{28}$$

Compared to the corresponding values (25) of the optimal protocol, the constant control protocol (26) behaves worse for smaller values of α, while both strategies behave similarly for large α. This is also evident in Fig. 2, where the conversion efficiency of protocol (26) is displayed as a function of the optical distance (blue dashed line).

As a specific example, we consider the case where $\alpha = 100$. Solving numerically transcendental Eq. (24), we obtain for the optimal protocol $\theta_0 \approx 1.540568$ rad. We subsequently use this
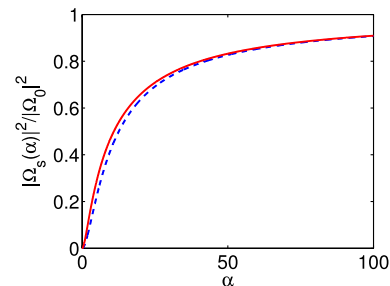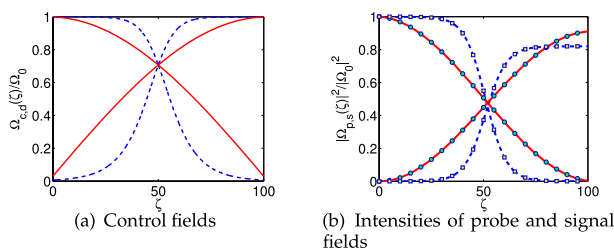

Fig. 2. Conversion efficiency for optimal protocol (red solid line) and constant control protocol of Eq. (26) (blue dashed line).

value in Eq. (22) and find $u_s \approx 0.015105$. The corresponding dimensionless spatially dependent control fields are displayed in Fig. 3(a) (red solid lines), as functions of the dimensionless distance $\zeta = z/L_{abs}$. In general, control field Ω_c precedes Ω_d in space, in order to prepare the necessary atomic coherences for the conversion Ω_p to Ω_s, but note that for the optimal protocol, $\Omega_d(0^+)$ and $\Omega_c(\alpha^-)$ have nonzero values, associated with the jumps in the mixing angle at $\zeta = 0$ and $\zeta = \alpha$, respectively. The corresponding dimensionless intensities of the probe and signal fields are plotted in Fig. 3(b), with red solid lines when using the approximate propagation Eq. (6) and with green circles for the full Maxwell–Bloch set of equations (without the weak loss assumption $\rho_{11} \approx 1$). Observe the very good agreement between the two results. For comparison, we consider a pair of adiabatic controls that we have used in Refs. [19,20,30],

$$\Omega_c = \Omega_0 \left[1 + e^{(\zeta - \zeta_0)/\bar{\zeta}}\right]^{-1/2}, \quad \Omega_d = \Omega_0 \left[1 + e^{-(\zeta - \zeta_0)/\bar{\zeta}}\right]^{-1/2}.$$

(29)

Here, we take $\zeta_0 = \alpha/2 = 50$ and $\bar{\zeta} = 5$, where the latter value is selected such that the adiabaticity condition $|\dot{\theta}| \ll 1/2 \Rightarrow \bar{\zeta} \gg 1/2$ is satisfied. The dimensionless control fields are plotted in Fig. 3(a) (blue dashed lines) as functions of the dimensionless distance $\zeta = z/L_{abs}$, and the corresponding dimensionless probe and signal pulses in Fig. 3(b), with blue dashed lines for the approximate propagation Eq. (6) and with yellow squares for the full Maxwell–Bloch equations. As before, a very good agreement is observed between the two results. The conversion efficiency at the final distance $\zeta = \alpha = 100$ for the adiabatic protocol (29) is 0.8197, much lower than the value 0.9094 obtained with the optimal protocol. The corresponding efficiency of the constant control protocol (26) is 0.9077, close to the optimal one, as shown in Fig. 2. For efficiency values close to one, we have to use larger values of α, a few hundred for the optimal protocol and about 1500–2000 for the adiabatic protocol. Note that in our recent work [19,20], using adiabatic controls in the direct configuration, we have reported a conversion efficiency close to unity for optical densities as small as $\alpha = 40$, but recently discovered that this result was overstated due to a scaling error.

In summary, we showed that for two frequently encountered configurations of the double-Λ atom–light coupling scheme, with the control fields applied in the same and different Λ-subsystems, the forward propagation of the probe and signal fields obeys the same set of equations. We also used optimal control theory to find the optimal spatially dependent control fields that maximize the conversion efficiency from the probe to the signal field, for a single-pass scheme and a specified optical density. Aside from this "optimal protocol" (20), we also considered two others, called the "constant control protocol" (26) and the "adiabatic protocol" (29).

See Supplement 1 for supporting content.

REFERENCES

1. M. D. Lukin, P. R. Hemmer, and M. O. Scully, Adv. At. Mol. Opt. Phys. **42**, 347 (2000).
2. O. Kocharovskaya and P. Mandel, Phys. Rev. A **42**, 523 (1990).
3. A. Raczyński, J. Zaremba, and S. Zielińska-Kaniasty, Phys. Rev. A **69**, 043801 (2004).
4. N. B. Phillips, A. V. Gorshkov, and I. Novikova, Phys. Rev. A **83**, 063823 (2011).
5. C. F. McCormick, V. Boyer, E. Arimondo, and P. D. Lett, Opt. Lett. **32**, 178 (2007).
6. M. T. Turnbull, P. G. Petrov, C. S. Embrey, A. M. Marino, and V. Boyer, Phys. Rev. A **88**, 033845 (2013).
7. H. Kang, G. Hernandez, J. Zhang, and Y. Zhu, Phys. Rev. A **73**, 011802 (2006).
8. X. Xu, S. Shen, and Y. Xiao, Opt. Express **21**, 11705 (2013).
9. A. J. Merriam, S. J. Sharpe, M. Shverdin, D. Manuszak, G. Y. Yin, and S. E. Harris, Phys. Rev. Lett. **84**, 5308 (2000).
10. H. Kang, G. Hernandez, and Y. Zhu, Phys. Rev. A **70**, 061804 (2004).
11. A. Eilam, A. D. Wilson-Gordon, and H. Friedmann, Phys. Rev. A **73**, 053805 (2006).
12. S. A. Moiseev and B. S. Ham, Phys. Rev. A **73**, 033812 (2006).
13. G. Wang, Y. Xue, J.-H. Wu, Z.-H. Kang, Y. Jiang, S.-S. Liu, and J.-Y. Gao, Opt. Lett. **35**, 3778 (2010).
14. C.-K. Chiu, Y.-H. Chen, Y.-C. Chen, I. A. Yu, Y.-C. Chen, and Y.-F. Chen, Phys. Rev. A **89**, 023839 (2014).
15. C.-Y. Lee, B.-H. Wu, G. Wang, Y.-F. Chen, Y.-C. Chen, and I. A. Yu, Opt. Express **24**, 1008 (2016).
16. Z.-Y. Liu, J.-T. Xiao, J.-K. Lin, J.-J. Wu, J.-Y. Juo, C.-Y. Cheng, and Y.-F. Chen, Sci. Rep. **7**, 15796 (2017).
17. J.-Y. Juo, J.-K. Lin, C.-Y. Cheng, Z.-Y. Liu, I. A. Yu, and Y.-F. Chen, Phys. Rev. A **97**, 053815 (2018).
18. H. R. Hamedi, J. Ruseckas, and G. Juzeliūnas, Phys. Rev. A **98**, 013840 (2018).
19. H. R. Hamedi, E. Paspalakis, G. Žlabys, G. Juzeliūnas, and J. Ruseckas, Phys. Rev. A **100**, 023811 (2019).
20. H. R. Hamedi, E. Paspalakis, G. Žlabys, G. Juzeliūnas, and J. Ruseckas, Phys. Rev. A **102**, 019903 (2020).
21. N. Prajapati, N. Super, N. R. Lanning, J. P. Dowling, and I. Novikova, Opt. Lett. **44**, 739 (2019).
22. L. Deng, M. G. Payne, G.-X. Huang, and E. W. Hagley, Phys. Rev. E **72**, 055601 (2005).
23. A. Eilam, A. D. Wilson-Gordon, and H. Friedmann, Opt. Lett. **33**, 1605 (2008).
24. Y.-F. Hsiao, P.-J. Tsai, C.-C. Lin, Y.-F. Chen, I. A. Yu, and Y.-C. Chen, Opt. Lett. **39**, 3394 (2014).
25. Z. Zhang, F. Wen, J. Che, D. Zhang, C. Li, Y. Zhang, and M. Xiao, Sci. Rep. **5**, 15058 (2015).
26. T. Jeong and H. S. Moon, Opt. Express **24**, 28774 (2016).
27. Z.-Y. Liu, Y.-H. Chen, Y.-C. Chen, H.-Y. Lo, P.-J. Tsai, I. A. Yu, Y.-C. Chen, and Y.-F. Chen, Phys. Rev. Lett. **117**, 203601 (2016).
28. A. E. Bryson, Jr. and Y.-C. Ho, *Applied Optimal Control: Optimization, Estimation, and Control* (Taylor & Francis Group, 1975).
29. M. Lapert, Y. Zhang, M. Braun, S. J. Glaser, and D. Sugny, Phys. Rev. Lett. **104**, 083001 (2010).
30. E. Paspalakis and Z. Kis, Opt. Lett. **27**, 1836 (2002).

(a) Control fields   (b) Intensities of probe and signal fields

Fig. 3. (a) Dimensionless control fields for the optimal protocol (red solid lines) and the adiabatic protocol (29) (blue dashed lines), as functions of the normalized distance $\zeta = z/L_{abs}$, for optical density $\alpha = 100$. (b) Propagation of the corresponding probe and signal pulses using the approximate Eq. (6) (red solid and blue dashed lines) and the full Maxwell–Bloch equations (green circles and yellow squares).